New Insights into the Defective Structure and Catalytic Activity of Pd/Ceria

J. A. Wang,*,† J. M. Dominguez,‡ A. Montoya,‡ S. Castillo,‡ J. Navarrete,‡ M. Moran-Pineda,‡ J. Reyes-Gasga,§ and X. Bokhimi§

Laboratorio de Catálisis y Materiales, SEPI-ESIQIE, Instituto Politécnico Nacional, Col. Zacatenco, Edificio 8, 3er Piso, 07738 Mexico D.F., Mexico, Programa de Ingeniería Molecular, Instituto Mexicano del Petróleo, Eje Central Lázaro Cárdenas No. 152, Delegación G. A. Madero, 07730 México D. F, Mexico, and Instituto de Física, Universidad Nacional Autonoma de México, A. P. 20-364, 01000 México D. F., Mexico

Received April 24, 2002. Revised Manuscript Received August 21, 2002

A surfactant-assisted synthesis method was applied to prepare nanosized ceria particles used as the three-way catalyst supports. The Rietveld refinements of crystalline structures of ceria calcined at various temperatures, together with XRD, FTIR, and TGA techniques, confirm that the surfactant cations are incorporated into the structural network of hydrous cerium oxide during the preparation stage, thus reducing the surface tension and diminishing the shrinkage of the mesoporous channels in the dried materials. The surface area is therefore enhanced but it provokes a significant distortion effect on the structure. It is evidenced by XRD analyses that a well-ordered cubic structure of ceria was formed at a temperature as low as 80 °C. The average crystallite size of ceria is determined by XRD within nanoscale range (i.e., 9−31 nm) when the calcination temperature increases from 80 to 800 °C, which is in good agreement with the data determined by TEM and electron diffraction methods. In addition, cationic defects are present in the crystalline structure of the solids, and the defect concentration in the unit lattice cell decreases as calcination temperature increases. CO chemisorption analysis by FTIR shows that CO may adsorb on Pd/ceria catalyst in different modes: linear Pd−CO and Ce^{4+}−CO bonds, bridged $Pd(CO)_2$ bonds, and multibonded $Pd_2(CO)_2$ bonds. CO adsorption might lead to CO_2 production from CO reacting with lattice oxygen and/or CO disproportionation catalyzed by palladium crystals. The CO oxidzed over the Pd supported catalysts makes it that T_{50} and T_{90} for the ceria prepared in the presence of surfactant diminish at 80 °C and 110 °C respectively, which are much lower than the ones prepared without surfactant, mainly due to its defective structure, enhanced surface area, and different CO adsorption behavior.

1. Introduction

Ceria and metal supported-ceria catalysts have been applied in defferent industrially catalytic processes such as de-SO_x and de-NO_x in FCC process, isomerization and oxidative dehydrogenation, and catalytic reforming of hydrocarbons.[1−5] One of the most important applications is as a key component of three-way catalysts, due to the property of ceria for storing or releasing oxygen under fuel-rich and oxygen-rich combustion conditions. Also, ceria supports are used for promoting the water−gas shift reaction, by stabilizing metal dispersion on its surface and thus avoiding its sintering.[6−11]

Most of the previous preparation methods of ceria use traditional techniques such as precipitation,[12] hydrothermal synthesis,[13] and sol−gel.[14] Though the sol−gel technique yields products with high purity, homogeneity, and well-controlled properties, the use of expensive organometallic compounds as precursors represents a disadvantage. Hence, a new synthetic approach becomes important. Alternatively, using supramolecular long-range ordered molecular aggregates of surfactants as templating agents, mesostructured aluminosilicates having high surface area were synthesized.[15] This

* To whom correspondence should be addressed. Tel: (52) 5 7296000, ext. 55124. Fax: (52) 5 5862728. E-mail: jwang@ipn.mx; or wang_j_a@yahoo.com.
† Instituto Politécnico Nacional.
‡ Instituto Mexicano del Petróleo.
§ Universidad Nacional Autonoma de México.

(1) Trovarelli, A. *Catal. Rev.-Sci. Eng.* **1996**, *38*, 439.
(2) Wang J. A.; Li, C. L. *J. Mol. Catal. A: Chem.* **1999**, *139*, 31.
(3) Guenin, M.; Da Siliva P. N.; Fréty, R. *Appl. Catal.* **1986**, *27*, 313.
(4) Yumaguchi, T.; Ikeda, N.; Hattori, H.; Tanae, K. *J. Catal.* **1981**, *67*, 324.
(5) Kennedy, E. M.; Cant, N. W. *Appl. Catal. A. Gen.* **1992**, *87*, 171.
(6) Crucq, A., Ed. *Catalysis and Automotive Polution Control II*; No. 71 in Studies in Surface Science and Catalysis Series; Elsevier: Amsterdam, The Netherlands, 1991.
(7) Fallah, J. E.; Boujana, S.; Dexpert, H.; Kiennemann, A.; Majeerus, J.; Touret, O.; Villain, F.; Le Normand, F. *J. Phys. Chem.* **1994**, *98*, 5522.
(8) Herz, R. K. *Ind. Eng. Chem. Prod. Res. Dev.* **1981**, *20*, 451.
(9) Shido, T.; Iwasawa,Y. *J. Catal.* **1992**, *136*, 493.
(10) Bera, P.; Patil, K. C.; Jayaram, V.; Subbanna, G. N.; Hegde, M. S. *J. Catal.* **2000**, *196*, 293.
(11) Ciuparu, D.; Bensalem, A.; Pfefferle, L. *Appl. Catal., B* **2000**, *26*, 241.
(12) Chen, P.-L.; Chen, I.-W. *J. Am. Ceram. Soc.* **1993**, *76*, 1577.
(13) Hirano, M.; Kato, E. *J. Am. Ceram. Soc.* **1996**, *79*, 777.
(14) Luo, M. F.; Lu, G. L.; Zheng, X. M. *J. Mater. Sci. Lett.* **1998**, *17*, 1553.

10.1021/cm020413u CCC: $22.00
Published on Web 10/24/2002

synthetic method makes it possible to synthesize new oxide mesoporous materials,[16−19] such as ZrO_2, TiO_2, and Nb_2O_5.[20−22] Recently, by using a hybrid organic route, the preparation of high-surface-area ceria with higher thermal stability was also reported, although a long-range ordered structure was not obtained.[23]

Textural properties of the cerium oxide seem dependent on the preparation methods. Some investigations have sought the relationship between the synthesis methods and surface and bulk structural properties,[23−25] but to date some questions still remain concerning the crystalline structure of ceria derived from supramecular templates and how it affects the formation of the lattice vacancies in ceria and its catalytic properties. In the present work, a surfactant-assisted synthesis method is applied to prepare ceria nanophases, to obtain high-surface-area materials and to further study the features of their crystalline structure and how these factors affect their catalytic activity. A multitechnique characterization by FTIR in situ, N_2 adsorption, XRD, TGA, and TEM was performed to have an insight of the structural and textural properties of the solids. Finally, the catalytic activity of CO oxidation over the P-supported ceria catalyst is reported.

2. Experimental Section

2.1 Sample Preparation. *2.2.1 Catalyst Support Synthesis.* In a typical preparation using a surfactant as structural director, 13.5 g of myristyltrimethylammonium bromide (referred to as C_{14}) was added in 500 mL of deionized water, then 50.5 g of $Ce(NO_3)_3{\cdot}6H_2O$ was dissolved in 500 mL of deionized water. The cerium solution was added dropwise to the surfactant solution with a proper agitation to disperse the droplets before local concentrations became excessive. Finally, the C_{14}/Ce mole ratio equal to 0.8 was obtained. The solution was stirred while additing ammonia (28%) to keep the pH at 11. Afterward, the slurry was continuously stirred for 4 h and then aged for 24 h at room temperature. The color of the mixture gradually changed from white to gray, and then to light yellow during the preparation. After this, filtering, and washing with water and mathanol followed until extra surfactants were removed from the solid (the sample is referred as $C_{14}-CeO_2$). The resulting materials were dried at 80 °C for 48 h and then were calcined at 200, 400, 600, and 800 °C for 4 h.

2.1.2 Catalyst Preparation. The 3 wt % $Pd/C_{14}-CeO_2$ catalysts were prepared by impregnating the ceria support with an aqueous solution of $Pd(NO_3)_2{\cdot}2H_2O$. The metal-supported catalysts were dried at 120 °C for several hours and then were calcined at 600 °C for 4 h. Before the catalytic test, all the samples were reduced under H_2 at 300 °C, for 2 h.

2.2 FT-IR Studies. The surface dehydroxylation and removal of the residual surfactants corresponding to the fresh samples were characterized by FTIR-in situ spectroscopy using a Nicolet Magna-IR 550 spectrometer fitted with gas lines vacuum and heating systems. The sample wafer placed in the IR cell was exposed in a N_2 flue with a rate of 20 mL/min. The IR spectra reported herein were recorded at 25, 100, 200, 300, 400, and 500 °C, respectively.

2.3 Measurements of Textural Properties. The textural properties of the solids such as specific surface area, pore volume, and pore size distribution were measured in a Digisorb 2600 sorptometer by means of N_2 physisorption isotherms at 78 K.

2.4 TG-DTG-FTIR Analysis. TG-DTG analyses were carried out in air using a Dupont model 950 thermoanalyzer from 25 to 800 °C at a heat rate of 20 °C/min to determine the weight loss stages during the thermal treatment and to estimate the amount of the cationic myristyltrimethylammoniumin incorporated with resulted materials. The gasous products produced during the TGA procedure were simultaneously monitored by means of on-line Fourier transfer infrared spectrometer.

2.5 CO Chemisorption. CO (99.9%) was introduced into a H-type adsorption cell containing 3 wt % Pd/ceria samples for CO chemisorption. Before adsorption the sample was thermally treated at 400 °C for 30 min to remove the impurities, then the adsorption cell was cooled to 200 °C, and the CO adsorption proceeded. After 15 min at 200 °C, the IR spectrum was recorded. Afterward, the temperature was reduced to 25 °C. To study the stability of the CO−Pd band at vacuum condition, the adsorption cell was evaluated. Before and after the evaluation, the IR spectra were recorded.

2.6 X-ray Diffraction and Rietveld Refinements. Powder X-ray diffraction data were collected at room temperature in a Siemens D-5000 diffractometer using $K_{\alpha\ L}\ Cu$ radiation and a secondary beam monochromator. The intensities were recorded within the 2θ from 20 to 110° with a step of 0.02° and a measuring time of 2.67 s each point. The crystalline structures were refined using the DBWS-9006 PC and WYRET programs.[26,27] The Rietveld refinement provided not only the concentration and average crystallite sizes of each phase present in the sample, but also provided the lattice point defects in the crystalline structures. The standard deviations, corresponding to the variation of the last significant figures, were given in parentheses.

2.7 TEM Observation. For TEM observation, a JEOL 100CX transmission microscope was used. The samples in powder were set in the surface of some cooper grids that were previously covered with a plastic film followed by a thin carbon film, according to the standard method to do this. Powder was deposited on the surface grid in a dry way. This method consists of putting the powder inside a syringe, covering the syringe entrance with a finger, and vigorously pulling the piston to create a powder cloud inside the syringe. After this, the grid was set in a clean surface and covered with the syringe's cylinder in such a way that the cloud particles were deposited over it.

2.8 Determination of Catalytic Activity. The CO oxidation test was carried out in a microreactor system with a catalyst laod of 50 mg. CO (8% N_2) mixed with air was fed into the reactor, with flow rates of CO and air of 20 mL/min and 40 mL/min, respectively. The effluent from the reactor was analyzed by on-line gas chromatography−IR analysis system equipped with a thermal conductivity detector. The conversion of CO to CO_2 over the catalysts was measured at various temperatures. T_{50} and T_{95} are defined as the temperatures at which the conversion of CO to CO_2 reached 50 and 95%, respectively.

(15) Raman, N. K.; Anderson, M. T.; Brinker, C. J. *Chem. Mater.* **1996**, *8*, 1682.
(16) Sayari, A., Jaroniec, M., Pinnavia T. J., Eds. *Nanoporous Materials II;* No. 129 in Studies of Surface Science and Catalysis; Elsevier, Amsterdam, 2000.
(17) Biz, S.; White, M. G. *J. Phys. Chem. B* **1999**, *103*, 8432.
(18) Behrens, P. *Angew. Chem., Int. Ed. Engl.* **1996**, *35* (5), 515.
(19) Huo, Q.; Margolese, D. I.; Ciesla, U.; Feng, P. T.; Gier, E.; Sieger, P.; Leon, R.; Petroff, P. M.; Schüth, F.; Stucky, G. D. *Nature* **1994**, *368*, 317.
(20) Huson, M. J.; Knowles, J. A. *J. Mater. Chem.* **1996**, *6* (1), 89.
(21) Redhakar, J. S.; Sayari, A. *Catal. Lett.* **1996**, *38*, 219.
(22) Antonelli, D. M.; Ying, J. *Angew. Chem.* **1996**, *108*, 461.
(23) Terribile, D.; Trovarelli, A.; De Leitenburg, C.; Dolcetti, G. *Chem. Mater.* **1997**, *9*, 2676.
(24) Liu, G.; Rodriguez, J. A.; Hrbek, J.; Dvorak, J.; Pend, C. H. F. *J. Phys. Chem. B* **2001**, *105*, 7762. (a) Garvie, L. A: J.; Buseck, P. R. *J. Phys. Chem. Solids* **1999**, *60*, 1943. (b) Prieto, C.; Lagarde, P.; Dexpert, H.; Briois, V.; Villain, F.; Verdaguer, M. *J. Phys. Chem. Solids* **1992**, *53*, 233.
(25) Fornasiero, P.; Kaspar, J.; Graziani, M. *Appl. Catal. B* **1999**, *22*, L11−L14.
(26) Young, R. A.; Sakthivel, A.; Moss, T. S.; Paiva-Santos, C. O. *J. Appl. Crystallogr.* **1995**, *28*, 366.
(27) Margarita Schneider EDV−Vertrieb, Sarnbergweg 18 D-8134, Pöcking, Germany, 1992, Tel: 0049−8157−8727, Fax: 0049−8157−4527.

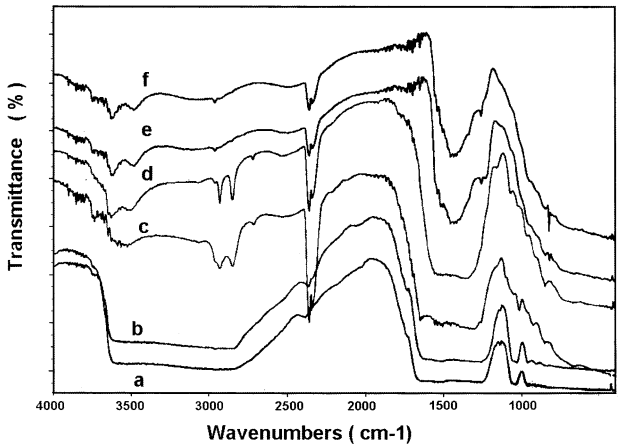

Figure 1. Set of FTIR-in situ spectra of the dried sample $C_{14}-CeO_2$ recorded at various temperatures: (a) 25 °C; (b) 100 °C; (c) 200 °C; (d) 300 °C; (e) 400 °C; and (f) 500 °C.

3. Results and Discussion

3.1 Surface Characterization by FTIR in situ. Figure 1 shows a set of FTIR-in situ spectra recorded at various temperatures from 25−500 °C. When the temperature rose from 25 to 100 °C, two very wide absorption peaks were observed in the regions between 3700 and 2500 cm^{-1}, as well as between 1700 and 1200 cm^{-1}. These peaks are due to water adsorbed on the surface of the solid and to the C−H bond corresponding to the surfactant. Another peak at 1050 cm^{-1} is likely due to the formation of the bridged carbonate-like species on the sample.[28,29] Below 1000 cm^{-1}, the absorption bands are assigned to Ce−O stretching bond.

When the in situ calcination temperature increased to 200 °C, the broad peak (3700−2500 cm^{-1}) was replaced by two group bands: one appearing at 3500 $cm^{-1}$and 3700 cm^{-1}, which respectively corresponded to the OH stretching frequency of unidentate Ce−OH and tridentate

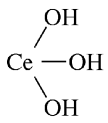

. The other double bands, in the range between 2900 and 2800 cm^{-1}, were assigned to the C−H stretching mode of hydrocarbon compounds.[30] The disappearance of the wide bands indicates that water is desorbed, and the presence of the C−H stretching absorption band indicates that some surfactant hydrocarbon chains are incorporated within the structural framework of the sample, even when the sample is calcined at 200 °C.

A very strong, sharp double band is located around 2300 cm^{-1}, which remarkably grows at 200 °C in comparison with the spectra recorded at 50 and 100 °C. These bands arise from the CO_2 absorption. The CO_2 signal arises from the decompostion of the residual organic surfactants, which confirms that the surfactants decompose to CO_2 around 200 °C.

The intensity of the bands appearing at 2800−2900 $cm^{-1}$and 2300 cm^{-1} diminishes as the calcination temperature increases to 300 °C, showing that the surfactants are progressively eliminated from the structure. The OH groups related to cerium ion as unidentate adsorption mode disappear, but other bands appear at 3600 cm^{-1}, which are assigned to bidentate OH stretching frequency of

The absorption bands at 1650 cm^{-1} are characteristic of the O−H bending vibration of the OH groups associated with adsorbed water. At 300 °C, the bands assigned to carbonate-like species at 1100 cm^{-1} diminish their intensity and decompose into CO_2 at this temperature.

When the temperature increases to 400 °C, the double bands at 2900−2800 cm^{-1} are almost removed, thus indicating that most of the surfactants burn off. However, a new band at 1490 cm^{-1} with a shoulder at 1300 cm^{-1} is observed. These bands are likely caused by the C−O and scissoring and rocking vibration of the C−H bonds of methylene groups or by a metal-nitrated bond associated with the surfactant.[31] Although most of the surfactants are removed, their decomposition might produce organic fragments that readsorb on the solid surface. In addition, other bands corresponding to hydroxyl ions are still observed at 500 °C. Therefore, the solid surface is not completely clean even at 500 °C. The FTIR-*extu* shows that adsorbed hydroxyls and the residual species could be completely removed at about 600 °C (not shown here).

3.2 Textural Properties. Table 1 shows the data of surface area, pore volume, and mean pore size of the $C_{14}-CeO_2$ which were calcined at different temperatures. For comparison, the textural data of a CeO_2 prepared without surfactant are also presented in Table 1. When the calcined temperature increases from 200 to 400 °C, the surface area of the $C_{14}-CeO_2$ sample increased from 112.2 to 121.3 m^2/g, and then it decreased as temperature increased from 400 to 800 °C. In contrast to this, the mean pore diameter shows a decrease, then an increase when the calcination temperature rises from 80 to 800 °C. Therefore, the changes of the surface area with the calcination temperature relate to changes of its pore diameter. However, the pore volume decreases linearly as the temperature increases.

The surface characterization by means of FTIR confirmed the existence of surfactant species incorporation in the network of the dried gel (Figure 1). The micellar rods of the sufactant in the pores of the solids give rise to progressive formation of the final mesostructured wall, reducing the shrinkage of the pores during the drying stage and thus enlarging the pore diameter in the dried gel. This is confirmed by the larger pore sizes shown in Table 1 (i.e., at 200 °C, D = 140 Å). When calcination temperature increases, the residual surfactants are gradually removed from the sample, thus

(28) Teribile, D.; Trovarelli, A.; Llorca, J.; De Leitenburg, C.; Dolcetti, G. *J. Catal.* **1998**, *178*, 299.

(29) Li, C.; Sakata, Y.; Arai, T.; Domen, K.; Maruya, K.; Onishi, T. *J. Chem. Soc., Faraday Trans.* **1989**, *185*, 929.

(30) Laachir, A.; Perrichon, V.; Badri, A.; Lamotte, J.; Catherine, E.; Lavalley, J.-C.; El Fallah, J.; Hilarer, L.; Le Normand, F.; Quéméré, E.; Sauvion, G. N.; Touret, O. *J. Chem. Soc., Faraday Trans.* **1991**, *87*, 1601.

(31) Nyquist, R. A.; Kagel, R. O. *Infrared of Inorganic Compounds*; Academic Press: New York, 1971; p 138.

Table 1. Textural Properties of the $C_{14}-CeO_2$ and $P-CeO_2$ Samples Calcined at Different Temperatures

	surface area (m^2/g)		pore volume (mL/g)		mean pore size (Å)	
temp. (°C)	$C_{14}-CeO_2$	$P-CeO_2$	$C_{14}-CeO_2$	$P-CeO_2$	$C_{14}-CeO_2$	$P-CeO_2$
200	112.2	67.8	0.3920	0.2985	140	118
400	121.3	69.2	0.3848	0.2843	127	120
600	79.9	34.7	0.3164	0.2534	158	125
800	36.5	17.9	0.2286	0.2080	250	264

provoking the decreasing of the pore size until most of the surfactants are removed, e.g. at 500 °C. Afterward the pore diameter starts increasing as the calcination temperature is higher than 600 °C, leading to decrease of surface area. This leads us to conclude that the presence of surfactants in the structure of the solid significantly influences their textural properties.

It is clearly shown that the surface area of $C_{14}-CeO_2$ is larger than that coresponding to the solids prepared without surfactant. It is known that during the precipitation stage, water molecules fill the internal pores to form hydrous metal oxides. When these are dried out, the capillary pressure at the liquld−vapor interface in the pores is produced, which stresses the metal oxide framework, thus provoking the collapse of the pore network, and in turn, reduces their surface area. However, as shown above by FTIR, in the case where surfactant is present (i.e., the myristyltrimethylammonium cations), they lead to interactions between the deprotonated hydroxyl groups and the positively charged surfactant headgroups, which may incorporate within the Ce−O−Ce framework, thus forming a polymeric nextwork of hydrous oxides such as $n CeO_x(O-\text{surfactant})_y \cdot m H_2O$.[23] Because the capillary pressure in the pores is generally proportional to the surface tension, and because the surfactant can reduce the water surface tension in the pores and thereby the gel shrinkage degree, a larger surface area and pore diameter of the solids prepared using the surfactant-assisted method is obtained.

The sorption isotherm of the samples at various temperatures is a type IV (not shown here). The hysteresis loop in the region of partial pressure from 0.4 to 0.9 of the isotherm is characteristic of framework mesoporosity. The lack of the typical step such as a sharp drop in the low P/P_0 range (i.e., $P/P_0 = 0.2$) in the adsorption isotherm as usually observed in the mesoporous materials, such as MCM-41, indicates that a relatively wide distribution of pore diameters is formed in ceria.

3.3 Thermal Analysis. The TGA profile exhibits several weight loss stages in the temperature range between 25 and 800 °C (Figure 2). The first stage leads to a 3.2 wt % weight loss below 150 °C, that was assigned to desorption of the adsorbed water. In the temperature range between 150 and 300 °C, there was a pronounced weight loss corresponding to 10.6 wt %. The third stage centered at about 458 °C produced a 3.1 wt % weight loss. Above 500 °C, the baseline slightly goes down, showing a weight loss less than 2 wt %.

Confirmations of gseous products corresponding to various weight losses in Figure 2 were obtained from the infared analysis. Figure 3 shows a set of FTIR spectra of the gaseous mixture discharged from the TGA system. In the beginning stage of the TG test (<50 °C), the IR spectrum exhibits only the baseline (Figure 3a), showing that the desorption of water or decomposing

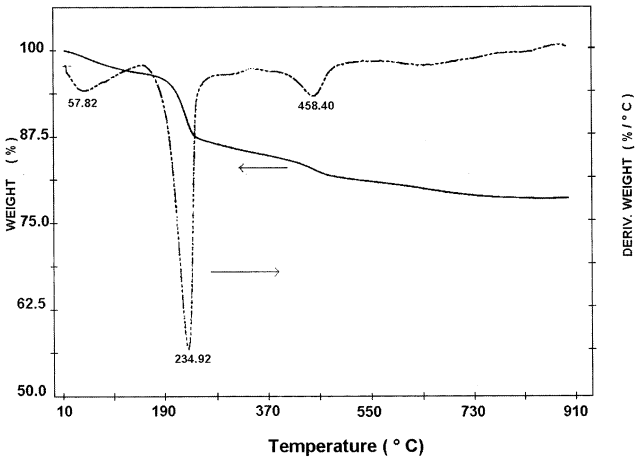

Figure 2. TG-DTG profile of the dried $C_{14}-CeO_2$ sample.

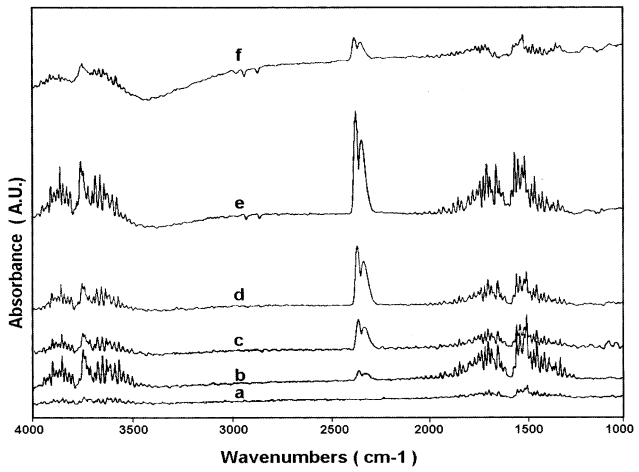

Figure 3. FTIR spectra of the exit gaseous mixture discharged from the TGA system: (a) 2 min; (b) 4 min; (c) 6 min; (d)10 min; (e) 42 min; and (f) 83 min.

of the surfactant did not yet occur. When the time increased from 3.2 to 9.3 min, which corresponds to a temperature interval between 60 and 150 °C, one group of peaks between 3900 and 3500 cm^{-1}, and another between 1700 and 1300 cm^{-1} were observed (Figure 3b−d); these are characteristic of molecular water. This comfirms that the first weight loss stage in the TG profile is caused by desorption of adsorbed water. However, it is noted that CO_2 was present in the exit steam as a double peak corresponding to CO_2 was found between 2400 and 2300 cm^{-1} in the IR spectra, and its instensity increased as the temperature increased. Because these two peaks were not observed in the beginning (Figure 3a), and the temperature for decomposition of the surfactant compounds seems too low, this CO_2 was likely produced by desorption of adsorbed CO_2 on the sample, because the sample was exposed in air and it could adsorb CO_2 on its surface.

In the second weight loss stage (150−250 °C), very sharp IR peaks corresponding to CO_2 and H_2O were

Table 2. Data Obtained from XRD and Electron Diffraction Experiments (CeO_2 Sample Was Prepared with Surfactant-Assisted Method and Calcined at 800 °C for 4 Hours)

JCPDS, $a = 5.42$ Å; $Fm3m$			XRD experiment		ED experiment	
d (Å)	int. (%)	hkl	2θ (°)	d (Å)	R (cm)	d (Å)
3.1234	100	111	14.4	3.08	0.8	3.04
2.7056	30	200	15.6	2.85	0.9	2.79
1.9134	52	220	23.9	1.92		
1.6318	42	311	28.25	1.64	1.6	1.62
1.5622	8	222	26.9	1.57		
1.3531	8	400	34.75	1.35		
1.2415	14	331	38.4	1.24	2.04	1.22
1.1048	14	422	44.2	1.10	2.26	1.11
1.0415	11	511	47.7	1.04	2.41	1.03
0.9147	13	531	57.4	0.92		
0.9019	6	600	58.6	0.90	2.8	0.90

Table 3. Atomic Fraction Coordinates of CeO_2 with Space Group *Fm*3*m*

atoms	positions	x	y	z
Ce	4a	0.000	0.000	0.000
O	8c	0.2500	0.2500	0.2500

identified (Figure 3e). This confirms that the largest weight loss in the TG profile is caused by both the decomposition of hydrous cerium oxide materials and surfactant decomposition.

In the third weight loss stage (440−470 °C), only CO_2 was identified (Figure 3f). This weight loss is likely resulted from the burn-off of the residual coke-like deposits produced by surfactant decomposition. The chemical composition of the related coke is very hydrogen-deficient as the IR band corresponded to water is very weak.

The prograssive shift of the baseline above 500 °C, might be due to the condensation of surface OH groups to form volatile water and/or the gradual combustion of some residual carbonaceous deposits.

3.4 Crystalline Structure Refinements. It is well-known that cerium forms two well-characterized oxides, CeO_2 and Ce_2O_3. An ideal CeO_2 crystal has a cubic, fluorite-type structure with space group $Fm3m$ where the cerium atom is at the center of a body-centered cube with eight oxygen atoms situated at the corners. Each cerium ion is octahedrally coordinated to eight oxygen ions and each oxygen anion is tetrahedrally coordinated to four cerium ions. There are four molecules per unit cell of CeO_2 crystal. The crystalline structure may show distortion when the lattice cerium ions (Ce^{4+}) are reduced to Ce^{3+} ions, however, the cubic structure can still be retained even when 30% CeO_2 is reduced to Ce_2O_3.[32] Therefore, to obtain actual structural information, the ceria structure was refined in the present study. All the atomic fractional coordinates were fixed during the refinement (Table 3). The XRD patterns and a Rietveld refinement plot are shown in Figures 4 and 5, respectively.

The XRD patterns of the solid dried at 80 °C, and those calcined at higher temperatures, exhibit complete reflections corresponding to cubic symmetry of CeO_2, thus indicating that a long-range cubic structure is formed even at 80 °C. This result differs from the report by Terribile and co-workers, where the ceria materials

(32) Wyckoff, R. W. G. *Crystal Structures*, Second Edition, Vol. 1; Roberet E. Krieger Publishing Company: Malabar, FL, 1982.

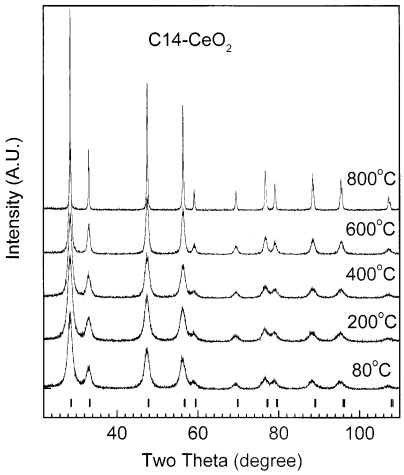

Figure 4. XRD patterns of the C_{14}−CeO_2 samples calcined at different temperatures.

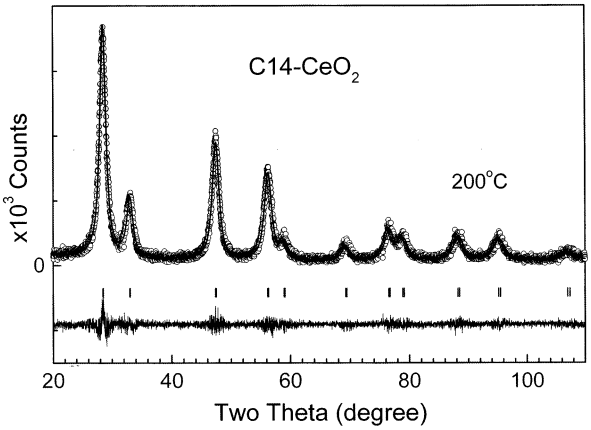

Figure 5. Rietveld plot of the sample C_{14}−CeO_2 calcined at 200 °C. Experimental data are indicated by circles, and the calculated curve obtained after the refinement is indicated with a continuous line. The tick marsks correspond to cubic phase. The continuous curve under the tick marks represents the difference between the experimental date and the calculated curve.

Table 4. Rietveld Refinement Results of C_{14}−CeO_2 Calcined at Different Temperatures

temp. (°C)	crystal size (Å)	lattice cell parameter (Å)	crystal strain $\langle\epsilon\rangle$ (%)
80	91.1 (1.1)	5.4226 (7)	1.1 (2)
200	90.1 (1.0)	5.4181 (7)	1.85 (0.16)
400	106.1 (1.4)	5.4129 (7)	2.0 (1)
600	148.3 (2.0)	5.4094 (5)	1.8 (1)
800	308.0 (4.5)	5.4091 (2)	0.65 (5)

calcined at 450 °C exhibited only a single broad reflection at low 2θ values in the XRD spectra, showing the absence of a long-range order in the structure.[23]

The crystallite size and lattice cell parameters in each sample were determined by means of the Rietveld refinements (Table 4). One observes that increasing the temperature from 80 to 800 °C provokes the crystallite size increasing from 9.1 to 30.8 nm. Concomitantly, the lattice cell parameters shows a slight contraction.

The ceria crystal contains microstrain which first increases as temperature increases from 80 to 400 °C, then decreases as temperature rises to 800 °C. The change of crystal strain is generally caused by structural distortion related to incorporation of foreign ions into the structure and calcination temperature. At temper-

Table 5. Cerium Atom Occupation and Cerium Defects in C_{14}−CeO_2

temp. (°C)	occupation number	defect concentration (%)	defect number per cell
80	0.0158 (0.1)	24.0	0.96
200	0.0166 (0.1)	20.2	0.81
400	0.0170 (0.1)	16.8	0.74
600	0.0173 (0.3)	18.3	0.68
800	0.0185 (0.1)	11.1	0.45

atures below 400 °C, the residual surfactants are gradually eliminated as the temperature increases, thus resulting in an increase of local microstrain within the crystal. When the calcination tempeature is higher than 400 °C, most of the surfactant molecules burn and their effect is significantly reduced. Therefore, the maximum value of the crystal strain, $\langle\epsilon\rangle = 2.0$, was achieved at 400 °C. As for the microstrain reduction at temperatures above 600 °C, it is likely due to more thermal energy supply that increases the lattice energy, thus diminishing the local microstrain.

The refinement of atomic occupancies in the structure shows that the samples calcined at different temperatures appear as cerium deficient, showing that the crystalline structure has cationic lattice defects (Table 5). This is the first report providing evidence of cationic lattice defect in the crystalline structure of CeO_2, which seems to contrast with the traditional idea that ceria is oxygen deficient (CeO_{2-x}), so that it is capable of storing oxygen in vacancies under the fuel-lean condition and releasing it under the fuel-rich condition.[33,6−10] This is interesting from both the academic and practical viewpoints, as it may require reconsideration of the mechanisms of oxygen storage and fast transferring in ceria.

For explaining the results of cationic defects, a model is assumed where some Ce^{3+} coexists with Ce^{4+} ions, to form Ce^{3+}/Ce^{4+} couples even in the oxidative condition on one hand, and some cerium lattice defects are created in the structure on the other hand. The existence of Ce^{3+} has been confirmed by other techniques such as XPS, photoemission spectroscopy, XANES, electron energy spectrocopy, and X-ray absorption spectrocopy.[24,34,35] Around the cationic defects, some oxygen ions are not fully bonded and then they are mobile compared to fully bonded ones. These lattice oxygen ions are active and they may be easily released when additional energy is supplied, thus forming free-like oxygen species. Existence of unfully bonded lattice oxygen ions in the defective stucture is a possible origin of the promotions of reducibility in zirconia−ceria solid solution. Therefore, the formation of these active oxygen ions seems favoring to the oxidation reaction under the fuel-rich condition in the three-way catalyst.

3.5 Morphological Features. Figure 6 shows the TEM image and electron diffraction pattern of the C_{14}−CeO_2 sample after calcining at 600 °C. The calculation data obtained from XRD and electron diffraction rings, together with the data cited from the JCPDS card, are reported in Table 2. The crystallite size is distributed in a narrow range between 10 and 20 nm, revealing that

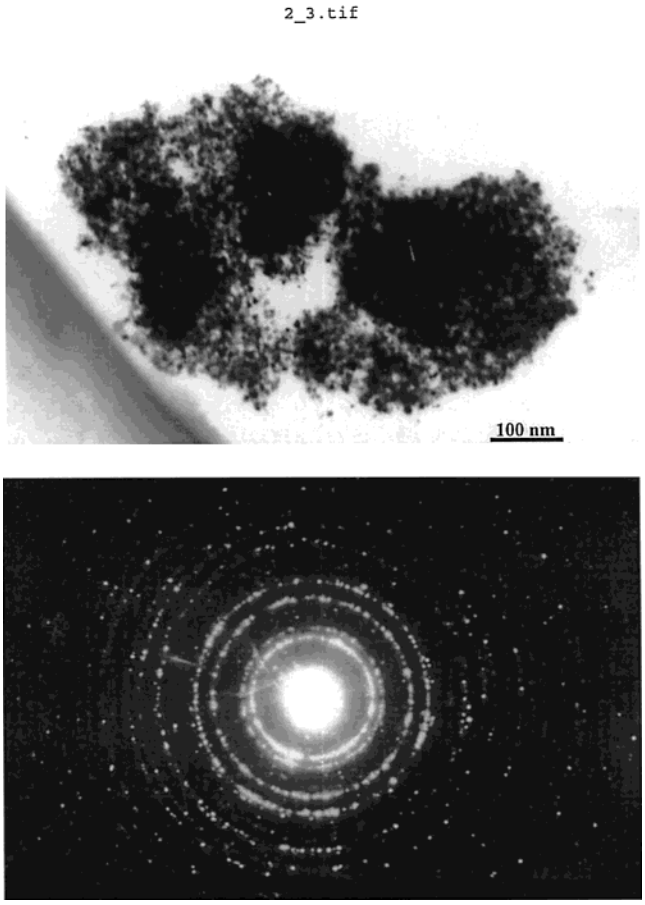

Figure 6. TEM images and electron diffraction of the C_{14}−ceria calcined at 600 °C: (a) TEM images and (b) electron diffraction patterns.

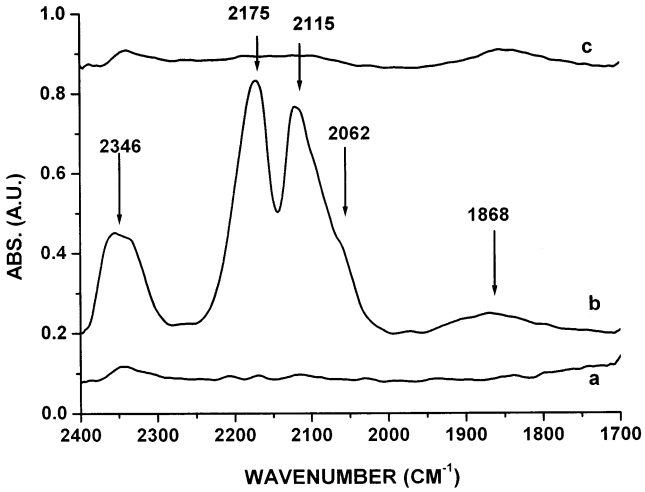

Figure 7. FTIR spectra of CO adsorption on the 3 wt % Pd/C_{14}−CeO_2 catalyst under various conditions: (a) before CO adsorption at 400 °C; (b) after CO adsorption at 200 °C for 10 min;and (c) after evacuating to 20 Pa at 25 °C.

the ceria crystals of the sample are highly homogeneous. The average crystallite size of ceria is about 15 nm observed by TEM, which is in good agreement with the value of 14.8 nm obtained from XRD anaysis and Rietveld refinement shown above.

3.6 CO Chemisorption. Figure 7 shows the FTIR spectra of CO adsorption on the Pd supported samples. The spectra were recorded at different conditions. Two groups of adsorption bands were observed: one group

(33) Yao, H. C.; Yao, Y.-F. Y. *J. Catal.* **1984**, *86*, 254.
(34) Garvie, L. A: J.; Buseck, P. R. *J. Phys. Chem. Solid* **1999**, *60*, 1943.
(35) Prieto, C.; Lagarde, P.; Dexpert, H.; Briois, V.; Villain, F.; Verdaguer, M. *J. Phys. Chem. Solids* **1992**, *53*, 233.

consisting of two peaks appeared at 2400−2280 cm^{-1} and another group contains three peaks which appeared between 2250 and 2000 cm^{-1}. In addition, a peak was formed in the range of 1800−1900 cm^{-1}.

In general, two adsorption modes of CO−Pd, linear and bridged bonds, can be observed in the case of CO adsorption on Pd atom clusters or crystals. The wavenumber of the CO−Pd linear bond and the bridged bond appears at the range of 2100−2000 cm^{-1} and 1800−2000 cm^{-1}, respectively.[36,37] On the basis of these assignments, the band appearing in 1800−2000 cm^{-1} was assigned to the bridged form of CO adsorption on 2-fold hollow sites of Pd atoms. The band at about 2115 cm^{-1} was assigned to CO linearly adsorbed on Pd crystallites. The band at 2175 cm^{-1} was mostly due to the adsorbed CO on cerium ions in a linear form on the support, similar to the observations reported in other work.[38,39]

It is noted that there is an absorption band appearing at 2062 cm^{-1} as a shoulder of the linear CO−Pd bond. It is suggested to be a multibonded CO on Pd atoms,[40,41] which is probably produced by the competitive adsorption of CO on palladium in linear and bridged modes. These three different adsorption modes of CO−metal are illustrated as follows:

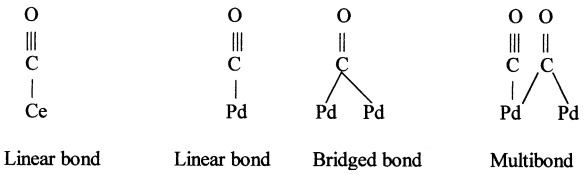

The twin bands in the region between 2400 and 2250 cm^{-1} are attributed to the adsorbed CO_2. As shown in the IR spectra, before exposure to CO environment, very weak bands corresponding to CO_2 were observed on the sample, indicating that a trace amount of CO_2 exists in the IR adsorption cell. Therefore, the observed CO_2 must be produced in the course of the CO adsorption procedure (Figure 6b). There are two possible pathways to produce CO_2: (i) CO reacting with lattice oxygen, and (ii) CO disproportionating to CO_2 and carbon. Because CO was introduced into the IR cell at 200 °C, the CO oxidation reaction easily takes place on the catalyst surface. This is supported by the catalytic test in a microreactor shown in the following section. Moreover, several reports have appeared regarding CO disproportionation where carbon deposits are detected after CO adsorption on the Pt/ceria, Pd/ceria, and other metals-supported ceria catalysts.[11,36,42,43] The Pd crystals are believed to catalyze the disproportionation reaction. Although we do not provide straightforward evidence concerning carbon formation in the present work, the possibility of CO disproportionation might be taken into account. After evaluating the adsorbed sample, the adsorbed CO_2 and linear-bonded CO were rapidly desorbed from the active sites, however, the bridged CO−Pd band was still observed (Figure 9c), indicating that stability of CO−metal bands is different.

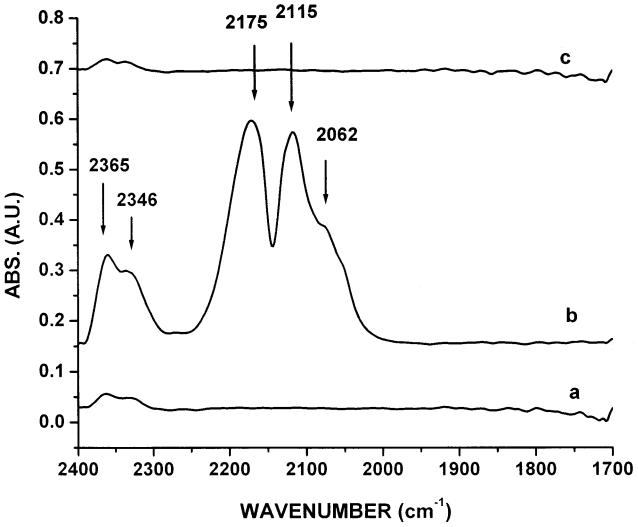

Figure 8. FTIR spectra of CO adsorption on the 3 wt % Pd/p−CeO_2 catalyst under various conditions: (a) before CO adsorption at 400 °C; (b) after CO adsorption at 200 °C for 10 min; and (c) after evacuating to 20 Pa at 25 °C.

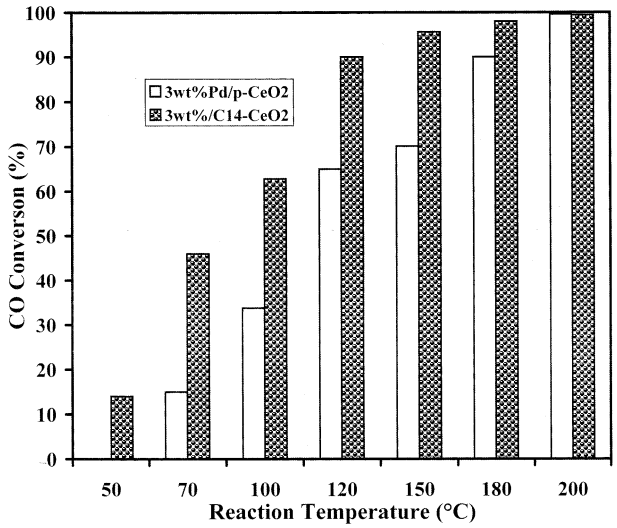

Figure 9. Catalytic activity of CO oxidation over the 3 wt % Pd/C_{14}−CeO_2 and 3 wt % Pd/p−CeO_2 catalysts.

Figure 8 shows the FTIR spectra of CO adsorption on Pd/p−CeO_2 solid. Compared to Figure 7, a difference of CO adsorption behavior between these two catalysts is found: no bridged CO−Pd bond is formed on the Pd/p−CeO_2 catalyst since no adsorption band was observed in the range 1800−1900 cm^{-1}.

3.7 CO Oxidation Activity. Figure 9 shows the catalytic activity of two Pd-supported ceria catalysts. Although the CO oxidation over these catalysts is complete at 200 °C, the light-off temperature is quite different, which is particularly important. When ceria prepared by using the surfactant-assisted technique is used as support, the catalyst shows very active CO oxidation at low temperature: its T_{50} and T_{90} were as

(36) Palazov, A.; Chang, C. C.; Kokes, R. J. *J. Catal.* **1975**, *36*, 338.
(37) Sheu, L. L.; Karpinski, Z.; Sachtler, W. M. H. *J. Phys. Chem.* **1989**, *93*, 4890.
(38) Holmgren, A.; Andersson, B.; Duprez, D. *Appl. Catal. B* **1999**, *22*, 215.
(39) Bozon-Verduraz, F.; Bensalem, A. *J. Chem. Soc., Faraday Trans.* **1994**, *190* (4), 653.
(40) Hoffmann, F. M. *Surf. Sci. Rep.* **1983**, *3*, 107.
(41) Arteaga, A.; Hoffmann, F. M.; Bradshaw, A. M. *Surf. Sci.* **1982**, *119*, 79.
(42) Pushkarev, V. V.; Kovalchuk, V. I. and D'Itri, J. L. *17th NACS Meeting*, June 3−8, 2001, Toronto, Canada, LP 4.
(43) Li, C.; Sakata, Y.; Arai, T.; Domen, K.; Maruya, K.; Onishi, T. *J. Chem. Soc. Chem. Commun.* **1991**, 410.

low as 80 and 110 °C. Particularly, at 50 °C, the conversion of CO oxidation over the $Pd/C_{14}-CeO_2$ reaches 13.9%, while the Pd supported on the precipitative ceria ($Pd/p-CeO_2$) shows no activity for CO oxidation at 50 °C. When the reaction increased to 100 °C, the $Pd/C_{14}-CeO_2$ catalyst achieved 62.4% conversion of CO, which is two times higher than that of the $Pd/p-CeO_2$ catalyst. These results reveal that CeO_2 prepared through the surfactant-assisted technique is superior to the one prepared by the precipitation method.

There are several possible reasons for the enhancement of catalytic activity of $Pd/C_{14}-CeO_2$ catalyst: first is its higher surface area. When $C_{14}-CeO_2$ was calcined at 600 and 800 °C, its surface area was, respectively, 79.5 and 36.5 m^2/g. However, at the same calcination temperature, the CeO_2 prepared by precipitation in the absence of surfactant shows only 34.7 m^2/g at 600 °C and 17.9 m^2/g at 800 °C; these are half of the values of $C_{14}-CeO_2$. The larger surface area and smaller crystalline size of C_{14}–ceria increase both the number of exposed cerium atoms and palladium metal dispersion. This is supported by the CO chemisorption measurement that metallic dispersion of 3% $Pd/C_{14}-CeO_2$ catalyst is 47%, but for 3% $Pd/C_{14}-CeO_2$ reaches only 24%. Second, CO can adsorb on the $Pd/C_{14}-CeO_2$ catalyst in both linear and bridged modes, however, on the $Pd/p-CeO_2$, no bridged bond can be formed. This difference may lead to catalytic activity of CO oxidation on the catalysts differing one from another. Next, as demonstrated above, there are some unfully bonded oxygen ions in bulk structure that related to cationic defects in the $C_{14}-CeO_2$ sample. These active oxygen ions in ceria lattice cells might move from bulk to surface, catalyzing CO oxidation. This suggestion indicates that the origin of generation of the oxygen mobility from bulk to surface is not only due to formation of oxygen vacanices on the catalyst surface during the reaction but also to existence of the unfully bonded oxygen lattices. Moreover, from the electronic point of view, because the *d*-band of Pd atoms is not totally occupied and these not unfully bonded oxygen ions in ceria show electron-rich character, it is possible that these oxygen ions donate their electrons to the vacancies of *d*-band of Pd atoms, modifying charge density around the Pd atoms. When CO adsorbed on this kind of Pd crystals, an enhancement of *d*-electrons from *4d* atomic orbital in Pd atoms back-donation to the $2\pi^*$-antibonding orbital of CO molecule occurs, which results in destabilization of the bond between CO and Pd atoms and activates the CO–Pd complex.[44–47] This also facilitates the CO oxidation.

4. Conclusions

A long-range mesostrutured nanoceria with enhanced surface area and uniform crystallite size was prepared through a surfactant-assisted technique in base media. FTIR characterization and XRD analyses reveal that the surfactant cation incorporated into the structural network could remain up to 500 °C, which gives rise to important effects on the structural distortion and surface area enhancement. Various modes of CO chemisorption on Pd/ceria catalyst were determined by FTIR; the observed CO_2 during CO adsorption probably resulted from both CO oxidation with lattice oxygen and CO disproportionation. For the first time, we report herein that cerium lattice defects exist in the crystalline structure and the defect concentration decreases with increasing of calcination temperature. This is of importance because it indicates that oxygen storage ability and fast oxygen mobility in ceria structure might relate to its cationic defects in the crystalline structure. Because of larger surface area, higher metal dispersion, and a defective structure, palladium-loaded ceria prepared by the surfactant-assisted method exhibits higher activity for CO complete oxidation with a lower light-off reaction temperature in comparison with the ceria prepared without surfactant.

Acknowledgment. The financial support from projects CONACyT-31282-U (Mexico) and FIES-98-29-III (IMP-IPN-Mexico) is acknowledged. J.A.W. thanks the scientific advisor fellowship in the Program of Molecular Engineering, Intsitute of Mexican Petroleum. The technical assistance of Y. M. Cerón (Instituto Politécnico Nacional, Mexico) in the sample preparation and A. Vázquez (Instituto Mexicano del Petróleo, Mexico) in the BET measurement is appreciated.

Supporting Information Available: Analytical data and isotherm plots (PDF). This material is available free of charge via the Internet at http://pubs.acs.org.

CM020413U

(44) Sachtler, W. M. H. *J. Catal.* **1974**, *32*, 315.
(45) Liu, R.; Tesche, B.; Knözinger, H. *J. Catal.* **1991**, *129*, 402.
(46) Rochefort, A.; Abon, M.; Delichere, P.; Bertolini, J. C. *Surf. Sci.* **1993**, *294*, 43.
(47) Wang, J. A.; Aguilar-Ríos, G.; Wang, R. *Appl. Surf. Sci.* **1999**, *147*, 44.